applied sciences

Article

Acoustic Equivalent Lasing and Coherent Perfect Absorption Based on a Conjugate Metamaterial Sphere

Xing-Xing Ma [1], Qi Wei [1,*], Xing-Feng Zhu [1,2], Jie Yao [1] and Da-Jian Wu [1,*]

[1] Jiangsu Key Laboratory of Opto-Electronic Technology, School of Physics and Technology, Nanjing Normal University, Nanjing 210023, China; 191002033@njnu.edu.cn (X.-X.M.); zhuxingfeng@njnu.edu.cn (X.-F.Z.); yaojie1@njnu.edu.cn (J.Y.)

[2] Key Laboratory of Modern Acoustics of MOE, School of Physics, Nanjing University, Nanjing 210093, China

* Correspondence: authors: weiqi@njnu.edu.cn (Q.W.); wudajian@njnu.edu.cn (D.-J.W.)

Abstract: Acoustic conjugate metamaterials (ACMs), in which the imaginary parts of the effective complex mass density and bulk compressibility are cancelled out in the refractive index, possess the elements of loss and gain simultaneously. Previous works have focused on panel ACMs for plane wave incidence. In this paper, we explore the extraordinary scattering properties, including the acoustic equivalent lasing (AEL) and coherent perfect absorption (CPA) modes, of a three-dimensional ACM sphere, where incident spherical waves with specific topological orders could be extremely scattered and totally absorbed, respectively. Theoretical analysis and numerical simulations show that the AEL or CPA mode with a single order can be realized with a small monolayer ACM sphere with appropriate parameters. A huge (relative to incident wavelength) ACM sphere with pure imaginary parameters could support the even- (or odd-) order AEL and odd- (or even-) order CPA modes simultaneously. In addition, the AEL and/or CPA with multiple orders could be realized based on a small multilayered ACM sphere. The proposed ACM sphere may provide an alternative method to design acoustic functional devices, such as amplifiers and absorbers.

Keywords: acoustic conjugate metamaterial; acoustic equivalent lasing; coherent perfect absorption

check for updates

Citation: Ma, X.-X.; Wei, Q.; Zhu, X.-F.; Yao, J.; Wu, D.-J. Acoustic Equivalent Lasing and Coherent Perfect Absorption Based on a Conjugate Metamaterial Sphere. *Appl. Sci.* **2022**, *12*, 1777. https://doi.org/10.3390/app12041777

Academic Editor: Claudio Guarnaccia

Received: 18 January 2022
Accepted: 7 February 2022
Published: 9 February 2022

1. Introduction

Acoustic metamaterials [1–10], composed of subwavelength structural units with specific designs, can exhibit almost arbitrary effective mass density and bulk compressibility, which not only greatly expand the variety of materials, but also enable the effective regulation of acoustic waves. In order to break through the limitations of conventional materials, acoustic metamaterials with negative and zero parameters have been studied extensively. Usually, negative acoustic parameters are attributed to specific resonances. For example, a cubic unit composed of a lead ball coated with silicone rubber can realize negative density when dipole resonances occur [1], while Helmholtz resonators can realize negative bulk compressibility when monopole resonances occur [4]. A negative effective density or bulk compressibility constitutes a single negative material [11–15], which can be used for acoustic insulation and noise reduction [16]. Acoustic waves cannot penetrate a single negative material but travel only along its surface due to the pure imaginary property of the refractive index. Combined with the negative density and bulk compressibility, a double negative material is formed [17–19], which can realize planar focusing, subwavelength imaging [20,21], and so on. Double negative materials can be realized, for example, by a system comprising two coupled membranes with two resonance modes (monopole and dipole) [22]. In addition, zero index materials have also been extensively studied [23–27], by which superreflection, total transmission, and cloaking can be realized. However, previous studies of acoustic metamaterials have focused on the real parts of acoustic parameters. It is also important to take the imaginary parts (indicating loss and gain of the materials) into account [28]. For example, a topological gallery insulator based on a gain medium enables the out-coupling of topological acoustic equivalent lasing (AEL) modes with the desired handedness [28], and nonreciprocity energy transmission can be realized by lossy materials [29–32].

A conjugate metamaterial, whose effective relative permittivity and permeability are complex conjugates of each other, was proposed in the field of electromagnetism more than a decade ago [33]. Based on the electromagnetic conjugate metamaterials, many excellent phenomena were realized, such as perfect absorption and amplification [34–36]. Inspired by this, acoustic conjugate metamaterials (ACMs) have recently been proposed, where the phases of the effective mass density and bulk compressibility are complex conjugates [37]. The ACMs possess a real refractive index, indicating the existence of undecaying propagating waves in the ACMs, although the materials exhibit the elements of gain and loss simultaneously. Based on an ACM slab, AEL and coherent perfect absorption (CPA) modes were realized for plane wave incidence. However, research on spherical ACMs has seldom been reported. In this paper, we explore the extraordinary scattering properties of a three-dimensional (3D) ACM sphere under spherical wave incidence with different topological orders. Analytical derivations with rigorous scattering theory and consistent simulations demonstrate that the AEL mode or (and) CPA mode, where incident spherical waves with specific topological orders are extremely scattered or (and) totally absorbed, could be realized with a small (huge) monolayer ACM sphere. Meanwhile, a multilayered ACM sphere is proposed to realize the AEL and/or CPA modes for spherical wave incidence with multiple orders.

This paper is organized as follows. In Section 2, we first propose an ACM sphere and build its scattering model. In Sections 3 and 4, we demonstrate the AEL and CPA modes, respectively, based on a small monolayer ACM sphere. In Section 5, we demonstrate the simultaneous realization of AEL and CPA modes based on a huge monolayer ACM sphere. In Section 6, a multilayered ACM sphere is proposed to realize the AEL and/or CPA modes with multiple orders. Section 7 contains a conclusion.

2. Scattering Model of an ACM Sphere

For an acoustic scattering system, where a scatterer couples to a discrete set of scattering channels (denoted as l), the harmonic pressure field outside the scatterer can be expressed as

$$p\left(\vec{r},t\right) = \sum_l \left[a_l p_l^{\text{in}}\left(\vec{r}\right) + b_l p_l^{\text{out}}\left(\vec{r}\right)\right] e^{-i\omega t}. \quad (1)$$

Here, ω is the angular frequency, $p_l^{\text{in}}\left(\vec{r}\right)$ and $p_l^{\text{out}}\left(\vec{r}\right)$ indicate the acoustic input and output l-th channel mode with proper analytic form. For a plane scatterer, the channel modes are plane waves, while for a cylindrical scatterer, they are cylindrical waves. The coefficients a_l and b_l are the complex amplitudes of the incoming and outgoing channel waves, which are further related by the scattering matrix S as

$$b_l = \sum_m S_{l,m} a_m, \quad (2)$$

where l and m denote scattering channels. It is noted that the scattering matrix S is symmetric, namely, $S_{l,m} = S_{m,l}$. The scattering matrix could describe the acoustic response of the scatterer under incidence. For example, by fine tailoring the acoustic parameters (including gain) and geometry of the scatterer, an eigenvalue of the scattering matrix could diverge at a real frequency, and the corresponding eigenstate indicates a solution with only outgoing waves, namely, a lasing mode [37]. Thus, the scattering system works as an acoustic equivalent laser at this frequency, which produces coherent outgoing waves with extensive intensities. The time-reversed counterpart to this lasing mode is a CPA mode [38–46], where the acoustic and geometric parameters of the scatterer are the same as those in the lasing mode, except that the gain is replaced with loss with equal magnitude. Here, an eigenvalue of the scattering matrix tends to zero at the same frequency for the lasing mode, and the corresponding eigenstate indicates a solution without outgoing waves. Now, the scattering system works as an acoustic coherent perfect absorber at this frequency, which could totally absorb a specific coherent incident wave pattern determined by the eigenstate. An acoustic system with effective loss (gain) could realize only the CPA (AEL) effect [38], while the simultaneous realization of AEL and CPA effects requires a system consisting of both gain and loss, which has been proposed based on an acoustic parity-time symmetric system [39] and an anti-parity-time symmetric system [40]. Besides, previous studies focused on one-dimensional (1D) and two-dimensional (2D) systems. In 1D systems, the AEL and CPA effects were demonstrated for plane normal incidence [39,40]. In a 2D panel system, such effects could be realized for plane oblique incidence [37]. In a 2D cylindrical system, the CPA effect was realized for cylindrical incidence with angular momentum [38]. In this work, we propose a multilayered ACM sphere to realize the AEL and CPA effects individually/simultaneously for spherical incidence.

Figure 1a,b show the diagram of the proposed multilayered ACM sphere in a 3D view and a cross section in the yz-plane, respectively. The multilayered ACM sphere is immersed in a conventional background medium (labeled as the zeroth region), whose mass density ρ_0 and bulk compressibility β_0 are both real and positive. The outer radius of the q-th layer (q = 1, 2, . . . , Q) of the ACM sphere is R_q, and each layer is characterized by the refractive index n_q and effective mass density ρ_q. The effective mass density ρ_q and bulk compressibility β_q for the q-th ACM layer are expressed as $\rho_q = |\rho_q|e^{i\alpha_q}$ and $\beta_q = |\beta_q|e^{-i\alpha_q}$, respectively, whose phases are complex conjugates of each other. Here, $|\rho_q|$ ($|\beta_q|$) denotes the amplitude of the effective mass density (bulk compressibility), α_q denotes a phase angle, and $n_q = \pm\sqrt{\rho_q\beta_q/\rho_0\beta_0}$ is the refractive index of the q-th ACM layer. For $0 < \alpha_q < \pi/2$ and $3\pi/2 < \alpha_q < 2\pi$, the sign "+" is taken, and the ACM features right-handedness (positive refractive index), while for $\pi/2 < \alpha_q < 3\pi/2$, the sign "−" is taken, and the ACM features left-handedness (negative refractive index). In particular, when $\alpha_q = \pi/2$ and $\alpha_q = 3\pi/2$, the ACM is called a pure imaginary metamaterial, and the material exhibits ambiguous handedness. When $\alpha_q = 0$ and $\alpha_q = \pi$, the ACM degenerates into double-positive and double-negative materials, respectively.

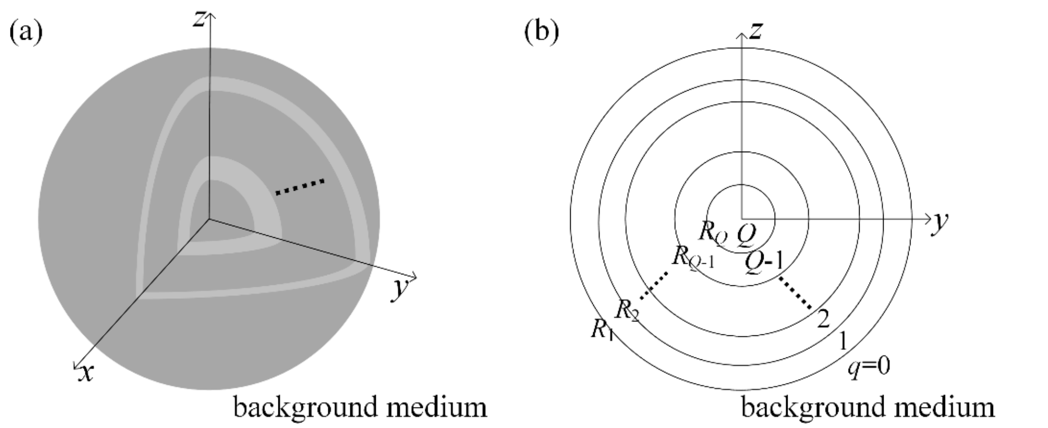

Figure 1. The diagram of a multilayered ACM sphere system: (**a**) a 3D view; (**b**) a cross section in the yz-plane.

Due to the spherical symmetry of the proposed ACM sphere, the channel modes used to describe the acoustic field distribution (see Equation (1)) are naturally spherical waves, which are a set of orthogonal separate variable solutions of the acoustic Helmholtz equation in spherical coordinates (r, θ, φ). Here, r, θ and φ denote the radius, angular and azimuthal angles in spherical coordinates, respectively. The case of axial symmetry is considered here, where the acoustic field is independent of coordinate φ. Therefore, for $0 \leq q \leq Q-1$, the total acoustic pressure in the q-th region can be expressed as

$$p_q(r,\theta) = \sum_{l=0}^{\infty} \left[a_q^l h_l^{(2)}(k_q r) + b_q^l h_l^{(1)}(k_q r) \right] P_l(\cos\theta). \tag{3}$$

Here, $h_l^{(1)}$ and $h_l^{(2)}$ are the spherical Hankel functions of the first and second kinds with the order l, and $P_l(\cos\theta)$ is the Legendre polynomial of order l, respectively. The parameter $k_q = n_q k_0$ denotes the wavenumber for the q-th region, in which $k_0 = 2\pi/\lambda_0$ is the wavenumber for the background medium and λ_0 is the wavelength in the background medium. The expressions $a_q^l h_l^{(2)}(k_q r) P_l(\cos\theta)$ and $b_q^l h_l^{(1)}(k_q r) P_l(\cos\theta)$ represent the incoming and outgoing channel spherical waves of order l in the q-th region, with a_q^l and b_q^l being the corresponding complex amplitudes. Here, the time variant item $e^{-i\omega t}$ is omitted for simplicity. The radial evolution of the spherical waves is given by the spherical Hankel functions, and the field evolution over θ is given by $P_l(\cos\theta)$.

Because of the orthogonality of the spherical waves, the continuity of acoustic pressure at the interface $r = R_q$ reads

$$h_l^{(1)}(k_{q-1}R_q) s_{q-1}^l - C_q^l a_q^l / a_{q-1}^l = -h_l^{(2)}(k_{q-1}R_q), \tag{4}$$

while the continuity of radial acoustic velocity at $r = R_q$ leads to

$$\eta_q h_l^{(1)'}(k_{q-1}R_q) s_{q-1}^l - \eta_{q-1} D_q^l a_q^l / a_{q-1}^l = -\eta_q h_l^{(2)'}(k_{q-1}R_q). \tag{5}$$

Here, $\eta_q = \rho_q / (n_q \rho_0)$ denotes the acoustic impedance of the q-th region relative to the background medium, the scattering coefficient $s_{q-1}^l = b_{q-1}^l / a_{q-1}^l$ is the ratio between the complex amplitudes of the outgoing and incoming spherical waves in the (q-1)-th region, $h_l^{(1)'}$ and $h_l^{(2)'}$ are the first-order derivatives of the corresponding spherical functions, $C_q^l = h_l^{(2)}(k_q R_q) + s_q^l h_l^{(1)}(k_q R_q)$, and $D_q^l = h_l^{(2)'}(k_q R_q) + s_q^l h_l^{(1)'}(k_q R_q)$, respectively. According to Equations (4) and (5), the scattering coefficient for the (q-1)-th region of order l can be obtained as

$$s_{q-1}^l = \frac{\eta_{q-1} D_q^l h_l^{(2)}(k_{q-1}R_q) - \eta_q C_q^l h_l^{(2)'}(k_{q-1}R_q)}{\eta_q C_q^l h_l^{(1)'}(k_{q-1}R_q) - \eta_{q-1} D_q^l h_l^{(1)}(k_{q-1}R_q)}. \tag{6}$$

Then, Equation (6) is a recursive formula that could apply to all $q \in [1,\ Q-1]$.

Since the spherical Hankel functions diverge at the origin, the acoustic pressure field in the Q-th region should be expressed as

$$p_Q(r,\theta) = \sum_{l=0}^{\infty} a_Q^l j_l(k_Q r) P_l(\cos\theta), \tag{7}$$

where a_Q^l is the complex amplitude of the penetrated channel spherical wave of order l, and j_l is the spherical Bessel function of the first kind with order l. By applying the continuous pressure and radial velocity boundary conditions at $r = R_Q$, the scattering coefficient in the ($Q-1$)-th region, i.e., s_{Q-1}^l, can be expressed as

$$s_{Q-1}^l = \frac{\eta_{Q-1} j'_l(k_Q R_Q) h_l^{(2)}(k_{Q-1}R_Q) - \eta_Q j_l(k_Q R_Q) h_l^{(2)'}(k_{Q-1}R_Q)}{\eta_Q j_l(k_Q R_Q) h_l^{(1)'}(k_{Q-1}R_Q) - \eta_{Q-1} j'_l(k_Q R_Q) h_l^{(1)}(k_{Q-1}R_Q)}. \tag{8}$$

Here, j_l' is the first-order derivative of j_l.

By iterating Equations (6) and (8), all scattering coefficients s_q^l ($q = 0, 1, \ldots, Q-1$) can be obtained. Similar to the process for solving the scattering coefficients, the transmission coefficient in the q-th region, i.e., a_q^l/a_{q-1}^l (q = 1, 2, . . . , Q), can be obtained accordingly by applying continuous boundary conditions. Then, the total acoustic field in the whole domain can be completely reconstructed from Equations (3) and (7) for a given incident pattern. Due to the orthogonality of the spherical channel waves, there is no interchannel scattering. According to Equation (2), therefore, the scattering matrix of the proposed ACM sphere system is diagonal with on-diagonal elements s_0^l, and the scattering coefficient s_0^l is also an eigenvalue of the scattering matrix for the proposed system. In the following, we focus on the extraordinary scattering properties of the ACM sphere by analyzing the scattering coefficient s_0^l.

3. AEL Based on a Small Monolayer Sphere

Let us start with the simplest case of a small monolayer ACM sphere, i.e., Q = 1. Then, the scattering coefficient of the monolayer ACM sphere can be obtained by taking Q = 1 into Equation (8), i.e.,

$$s_0^l = \frac{j'_l(k_1R_1)h_l^{(2)}(k_0R_1) - \eta_1 j_l(k_1R_1)h_l^{(2)'}(k_0R_1)}{\eta_1 j_l(k_1R_1)h_l^{(1)'}(k_0R_1) - j'_l(k_1R_1)h_l^{(1)}(k_0R_1)}. \tag{9}$$

The AEL mode corresponds to a divergent eigenvalue of the scattering matrix, namely, a divergence scattering coefficient s_0^l for the proposed system. Therefore, the condition for the AEL mode, which could generate a strong spherical wave with the order l, can be concluded from the zero of the denominator of Equation (9), namely

$$\frac{h_l^{(1)}(k_0R_1)}{h_l^{(1)\prime}(k_0R_1)} = \exp(i\alpha_1)\frac{|\rho_1|}{|n_1|\rho_0}\frac{j_l(|n_1|k_0R_1)}{j_l'(|n_1|k_0R_1)}. \tag{10}$$

For simplicity, we define $A_l(|n_1|) = j_l(|n_1|k_0R_1)/j_l'(|n_1|k_0R_1)$ and $B_l = h_l^{(1)}(k_0R_1)/h_l^{(1)'}(k_0R_1)$, so Equation (10) can be simplified to

$$B_l = \exp(i\alpha_1)|\rho_1|A_l(|n_1|)/(\rho_0|n_1|). \tag{11}$$

The function A_l is the ratio of the spherical Bessel function of the first kind to its derivative and therefore is real, while B_l is the ratio of the spherical Hankel function of the first kind to its derivative, which is complex. Thus, Equation (11) can be further expressed as

$$\exp(i\phi_l)\xi_l = \exp(i\alpha_1)|\rho_1|A_l(|n_1|)/(\rho_0|n_1|), \tag{12}$$

where ξ_l and ϕ_l are the amplitude and phase of B_l, respectively. There are two kinds of solutions for Equation (12), denoted as:

$$\alpha_1 = \phi_l,\ A_l(|n_1|) = \rho_0|n_1|\xi_l/|\rho_1|, \tag{13}$$

$$\alpha_1 = \phi_l + \pi,\ A_l(|n_1|) = -\rho_0|n_1|\xi_l/|\rho_1|. \tag{14}$$

If the amplitude of the mass density $|\rho_1| = |n_1|\rho_0$ is taken for the ACM sphere, the acoustic parameters of the ACM sphere are simply determined by the phase angle α_1 and n_1, and Equations (13) and (14) can be rewritten as

$$\alpha_1^{\mathrm{L}} = \phi_l,\ A_l\left(\left|n_1^{\mathrm{L}}\right|\right) = \xi_l, \tag{15}$$

$$\alpha_1^{\mathrm{L}} = \phi_l + \pi,\ A_l\left(\left|n_1^{\mathrm{L}}\right|\right) = -\xi_l. \tag{16}$$

Here, α_1^{L} and n_1^{L} satisfying Equations (15) and (16) represent the particular phase angle and refractive index of the monolayer ACM sphere, respectively, leading to the AEL mode, where the ACM sphere could generate a strong spherical wave with the order l at a given working frequency.

Figure 2a,b show the phase ϕ_l and amplitude ξ_l of B_l (see Equation (12)) versus R_1, in which black solid, red dashed, and blue dotted curves correspond to l = 0, 1, and 2, respectively. For $R_1 = 0.35\lambda_0$, $\phi_0 = -0.6358\pi$, $\phi_1 = -0.6818\pi$, and $\phi_2 = -0.8170\pi$ (see Figure 2a); $\xi_0 = 0.9103$, $\xi_1 = 1.0151$, and $\xi_2 = 1.0901$ (see Figure 2b). Therefore, some values of α_1^{L} and n_1^{L} can be found to realize the AEL mode when $R_1 = 0.35\lambda_0$. Taking l = 0 as an example, Figure 2c shows the A_l for l = 0 versus the refractive index $|n_1|$. The values of $\left|n_1^{\mathrm{L}}\right|$ that lead to the AEL mode for l = 0 can be found to search the intersections of ξ_0 (or $-\xi_0$) (black dashed lines) and A_0 (black solid curves). For example, for l = 0, $\alpha_1^{\mathrm{L}} = -0.6358\pi$ and $\left|n_1^{\mathrm{L}}\right| = 1.7163$ satisfy Equation (15); $\alpha_1^{\mathrm{L}} = 0.3642\pi$ and $\left|n_1^{\mathrm{L}}\right| = 0.9698$ satisfy Equation (16). Similarly, when l = 1, $\alpha_1^{\mathrm{L}} = -0.6818\pi$ and $\left|n_1^{\mathrm{L}}\right| = 2.3674$ for Equation (15); $\alpha_1^{\mathrm{L}} = 0.3182\pi$ and $\left|n_1^{\mathrm{L}}\right| = 1.5894$ for Equation (16). When l = 2, $\alpha_1^{\mathrm{L}} = -0.8170\pi$ and $\left|n_1^{\mathrm{L}}\right| = 2.9715$ for Equation (15); $\alpha_1^{\mathrm{L}} = 0.1830\pi$ and $\left|n_1^{\mathrm{L}}\right| = 2.1567$ for Equation (16). It is worth noting that Equations (15) and (16) have more solutions with larger $\left|n_1^{\mathrm{L}}\right|$ due to oscillatory properties of the function A_l for a fixed order l.

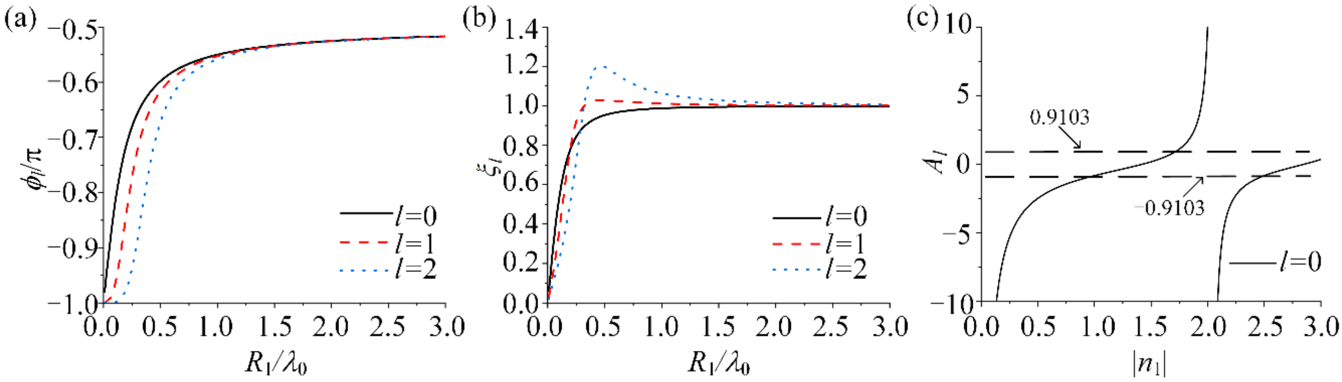

Figure 2. (**a**) Phase ϕ_l and (**b**) amplitude ξ_l of B_l versus radius R_1/λ_0. Black solid, red dashed, and blue dotted curves correspond to l = 0, 1, and 2, respectively. (**c**) The function A_l versus the refractive index $|n_1|$ for l = 0.

The AEL modes are further numerically simulated by using the finite element method based on the above analytical derivations. Figure 3 shows the total acoustic pressure fields in the yz-plane for spherical wave with an order l impinging on an ACM sphere with particular acoustic parameters, in which Figure 3a–c correspond to l = 0, 1 and 2, respectively. Without loss of generality, the background medium is set as air with the mass density ρ_0 = 1.21 kg/m^3 and the bulk compressibility $\beta_0 = 1/\rho_0 c_0^2$ in all simulations. Here, the sound speed of air c_0 = 343 m/s. The incidence wavelength is set as $\lambda_0 = 1$ m, and the distribution of the incident pressure field at the outer simulation boundary ($r = \lambda_0$) is set to $P_l(\cos\theta)$. The inner black circles in the figures denote the outer radius of the ACM sphere ($R_1 = 0.35\lambda_0$). For l = 0 (Figure 3a), $\alpha_1^{\mathrm{L}} = -0.6358\pi$ and $\left|n_1^{\mathrm{L}}\right| = 1.7163$ are taken to realize the AEL mode. Similarly, for l = 1 (Figure 3b), $\alpha_1^{\mathrm{L}} = -0.6818\pi$ and $\left|n_1^{\mathrm{L}}\right| = 2.3674$ are taken, while for l = 2 (Figure 3c), $\alpha_1^{\mathrm{L}} = -0.8170\pi$ and $\left|n_1^{\mathrm{L}}\right| = 2.9715$ are taken. For l = 0, the acoustic field distribution shows the shape of concentric circles and is completely determined by the coordinate r; when l = 1, the acoustic intensity along the z-axis is the strongest, and the field is symmetric about the z-axis; when l = 2, the maximum of the acoustic intensity is distributed along the y-axis and z-axis, and the acoustic field is symmetrical about the y-axis and z-axis. In all cases, the total acoustic pressure fields are very intense (see color bars) relative to the incidence. Therefore, the AEL mode is successfully realized based on an ACM sphere with appropriate parameters, where a strong spherical wave with the desired order l is scattered.

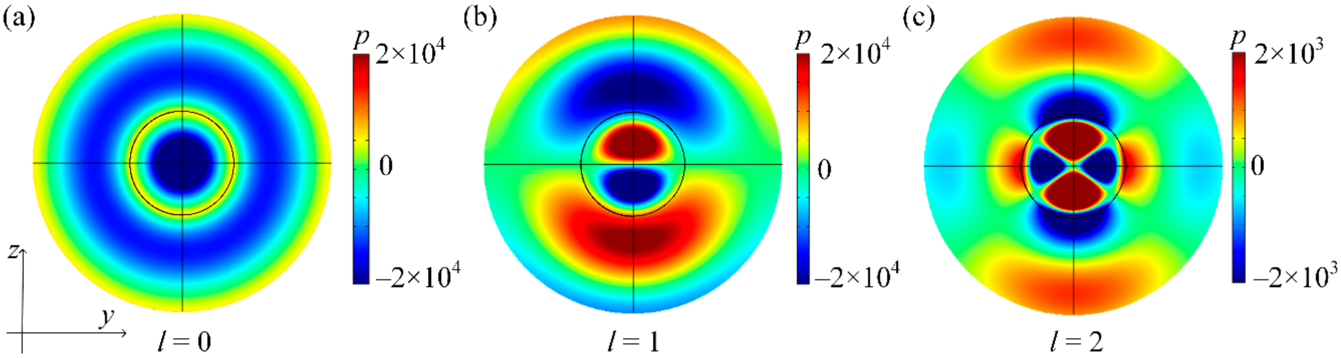

Figure 3. Simulated total acoustic pressure fields of the AEL modes in the yz-plane for spherical wave incidence with order l. (**a**) $l = 0$, $\alpha_1^{\mathrm{L}} = -0.6358\pi$, and $|n_1^{\mathrm{L}}| = 1.7163$. (**b**) $l = 1$, $\alpha_1^{\mathrm{L}} = -0.6818\pi$, and $|n_1^{\mathrm{L}}| = 2.3674$. (**c**) $l = 2$, $\alpha_1^{\mathrm{L}} = -0.8170\pi$, and $|n_1^{\mathrm{L}}| = 2.9715$. In all simulations, $R_1 = 0.35\lambda_0$, $\lambda_0 = 1$ m, and the distribution of the incident pressure field at the outer simulation boundary ($r = \lambda_0$) is $P_l(\cos\theta)$.

4. CPA Based on a Small Monolayer Sphere

In contrast to the AEL mode, the CPA mode corresponds to a vanishing eigenvalue of the scattering matrix, namely, a vanishing scattering coefficient s_0^l for the proposed system. Then, the incident spherical wave with the order l could be fully absorbed without any scattered waves. Therefore, the condition for the CPA mode can be concluded from the zero of the numerator of Equation (9), namely

$$\frac{h_l^{(2)}(k_0R_1)}{h_l^{(2)\prime}(k_0R_1)} = \exp(i\alpha_1)\frac{|\rho_1|}{|n_1|\rho_0}\frac{j_l(|n_1|k_0R_1)}{j_l'(|n_1|k_0R_1)}. \tag{17}$$

By numerically solving Equation (17), based on a similar procedure for solving Equation (10), one can obtain a series phase angle (α_1^{C}) and refractive index (n_1^{C}) solutions for realizing the CPA mode with the desired order l at a given working frequency. It is worth pointing out that Equations (10) and (17) have the same form but different kinds of spherical Hankel functions. Due to the complex conjugate nature between the first and second kinds of spherical Hankel functions, for the same radius R_1, the solutions (α_1^{C}, n_1^{C}) of Equation (17) have a special relationship with that (α_1^{L}, n_1^{L}) of Equation (10), namely

$$\alpha_1^{\mathrm{C}} = -\alpha_1^{\mathrm{L}},\ \left|n_1^{\mathrm{C}}\right| = \left|n_1^{\mathrm{L}}\right|. \tag{18}$$

On the other hand, the CPA mode could be regarded as a time reversal counterpart of the lasing [40–45]. Therefore, an AEL mode always corresponds to a CPA mode where the acoustic constitutive parameters of the two modes are complex conjugates. For the proposed ACM sphere, the complex conjugate acoustic parameters directly lead to Equation (18). In the following, instead of directly solving Equation (17), we employ the particular parameters (α_1^{L}, n_1^{L}) for achieving the AEL (see previous section), together with Equation (18) to obtain the parameter solutions (α_1^{C}, n_1^{C}) for achieving the CPA.

Figure 4 shows the simulated total acoustic pressure fields in the yz-plane where spherical waves with orders $l = 0$, 1, and 2 are incident on ACM spheres with particular acoustic parameters, respectively. The radii (R_1) for all ACM spheres are $0.35\lambda_0$, with $\lambda_0 = 1$ m as the incidence wavelength, and the distribution of the incident pressure field at the outer simulation boundary ($r = \lambda_0$) is set as $P_l(\cos\theta)$. In the case of $l = 0$ (Figure 4a), $\alpha_1^{\mathrm{C}} = 0.6358\pi$ and $|n_1^{\mathrm{C}}| = 1.7163$ are taken to realize the CPA mode. Similarly, for $l = 1$ (Figure 4b), $\alpha_1^{\mathrm{C}} = 0.6818\pi$ and $|n_1^{\mathrm{C}}| = 2.3674$; for $l = 2$ (Figure 4c), $\alpha_1^{\mathrm{C}} = 0.8170\pi$ and $|n_1^{\mathrm{C}}| = 2.9715$. In other words, all the simulation parameters in Figures 3 and 4 are the same, except that the acoustic parameters of the ACM spheres in Figure 4 are complex conjugates with those in Figure 3.

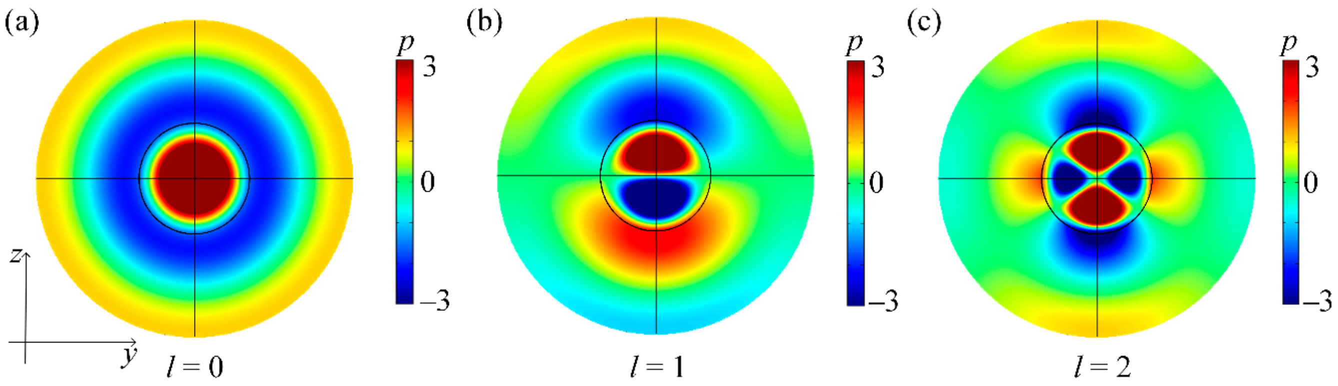

Figure 4. Simulated total acoustic pressure fields of the CPA modes in the *yz*-plane for spherical wave incidence with order l. (**a**) $l = 0$, $\alpha_1^C = 0.6358\pi$, and $|n_1^C| = 1.7163$. (**b**) $l = 1$, $\alpha_1^C = 0.6818\pi$, and $|n_1^C| = 2.3674$. (**c**) $l = 2$, $\alpha_1^C = 0.8170\pi$, and $|n_1^C| = 2.9715$. In all simulations, $R_1 = 0.35\lambda_0$, $\lambda_0 = 1$ m, and the distribution of the incident pressure field at the outer simulation boundary ($r = \lambda_0$) is $P_l(\cos\theta)$.

In contrast to the AEL modes (Figure 3), the acoustic fields in Figure 4 are weak (see color bars). Quantitatively, the values of the total fields at the outer simulation boundary are very close to $P_l(\cos\theta)$, respectively, which are equal to the incident pressure. Meanwhile, when $l = 0$, the acoustic field presents the shape of concentric circles. When $l = 1$ (2), the acoustic field is symmetric about the z-axis (y-axis and z-axis). The field profiles outside the spheres maintain the shapes of 0th-order, 1st-order, and 2nd-order spherical waves, respectively, and no obvious interference pattern is observed. The incident spherical waves with desired order l are thus totally absorbed without any scattering. Therefore, the CPA modes for spherical wave incidence with the order l are realized based on the ACM sphere with appropriate parameters.

5. Simultaneous AEL and CPA Based on a Huge Monolayer Sphere

In the previous sections, it was demonstrated that by fine modulating the acoustic and geometric parameters of a small monolayer ACM sphere, an AEL or CPA mode with order l could be realized at a working frequency. In this section, we will show that a huge monolayer ACM sphere can support the AEL and CPA modes simultaneously. When R_1 is far beyond the incidence wavelength λ_0, i.e., $R_1 \gg \lambda_0$, the phases ϕ_l of B_l for all orders l approach $-\pi/2$ (see Figure 2a), and the amplitudes ξ_l of B_l approach 1 (see Figure 2b). Therefore, when $R_1 \gg \lambda_0$, together with $|\rho_1| = |n_1|\rho_0$, the condition to realize the AEL mode (see Equations (15) and (16)) can be written as

$$\alpha_1^L = -\pi/2,\ A_l\left(\left|n_1^L\right|\right) = 1, \tag{19}$$

$$\alpha_1^L = \pi/2,\ A_l\left(\left|n_1^L\right|\right) = -1. \tag{20}$$

Furthermore, when $R_1 \gg \lambda_0$, the function $A_l(|n_1|)$ will approach

$$A_l(|n_1|) \to \tan(|n_1|k_0R_1)\ (\text{for even } l), \tag{21}$$

$$A_l(|n_1|) \to -\cot(|n_1|k_0R_1)\ (\text{for odd } l). \tag{22}$$

Therefore, for even-order l, the condition to realize the AEL mode can be expressed as

$$\alpha_1^L = -\pi/2,\ \tan\left(\left|n_1^L\right|k_0R_1\right) = 1, \tag{23}$$

$$\alpha_1^L = \pi/2,\ \tan\left(\left|n_1^L\right|k_0R_1\right) = -1, \tag{24}$$

while that for odd order l is

$$\alpha_1^{\mathrm{L}} = -\pi/2,\ \cot\left(\left|n_1^{\mathrm{L}}\right|k_0R_1\right) = -1, \tag{25}$$

$$\alpha_1^{\mathrm{L}} = \pi/2,\ \cot\left(\left|n_1^{\mathrm{L}}\right|k_0R_1\right) = 1. \tag{26}$$

According to Equation (18), for even-order l, the corresponding CPA mode condition can be expressed as

$$\alpha_1^{\mathrm{C}} = \pi/2,\ \tan\left(\left|n_1^{\mathrm{C}}\right|k_0R_1\right) = 1, \tag{27}$$

$$\alpha_1^{\mathrm{C}} = -\pi/2,\ \tan\left(\left|n_1^{\mathrm{C}}\right|k_0R_1\right) = -1, \tag{28}$$

while that for odd order l is

$$\alpha_1^{\mathrm{C}} = \pi/2,\ \cot\left(\left|n_1^{\mathrm{C}}\right|k_0R_1\right) = -1, \tag{29}$$

$$\alpha_1^{\mathrm{C}} = -\pi/2,\ \cot\left(\left|n_1^{\mathrm{C}}\right|k_0R_1\right) = 1. \tag{30}$$

Comparing Equations (23)–(26) and (27)–(30), when $\alpha_1 = -\pi/2$ ($\alpha_1 = \pi/2$) and $\tan(|n_1|k_0R_1) = \cot(|n_1|k_0R_1) = 1$ [$\tan(|n_1|k_0R_1) = \cot(|n_1|k_0R_1) = -1$], the large ACM sphere will extremely amplify spherical waves with all even orders l and totally absorb spherical waves with all odd orders l simultaneously. In contrast, when $\alpha_1 = -\pi/2$ ($\alpha_1 = \pi/2$) and $\tan(|n_1|k_0R_1) = \cot(|n_1|k_0R_1) = -1$ [$\tan(|n_1|k_0R_1) = \cot(|n_1|k_0R_1) = 1$], the large ACM sphere will extremely amplify spherical waves with all odd orders l and perfectly absorb spherical waves with all even orders l.

Figure 5a,b show $A_l(|n_1|)$ with l = even and l = odd, respectively, in which $R_1 = 100\lambda_0$. Some values of $|n_1|$ can be found to realize the coexistence of the AEL and CPA modes. For example, if $|n_1| = 1.0112$, $A_l = 1$ for even l and $A_l = -1$ for odd l. In this case, if the phase α_1 of the ACM sphere is further set as $-\pi/2$ ($\pi/2$), the AEL (CPA) mode occurs for all even orders l, and the CPA (AEL) mode occurs for all odd orders l. Similarly, if $|n_1| = 1.0187$, $A_l = -1$ for even l, and $A_l = 1$ for odd l. In this case, by further setting the phase α_1 of the ACM sphere as $-\pi/2$ ($\pi/2$), it could realize the CPA (AEL) mode for all even orders l and the AEL (CPA) mode for all odd orders l. Figure 5c,d show the scattering coefficient $\left|s_0^l\right|$ for orders from 0 to 5 when $|n_1| = 1.0112$ and $|n_1| = 1.0187$, respectively, in which $\alpha_1 = -\pi/2$ and $R_1 = 100\lambda_0$. Figure 5c,d show that $\left|s_0^l\right|$ tends to zero for l = 1, 3 and 5 (l = 0, 2 and 4) and tends to large values for l = 0, 2 and 4 (l = 1, 3 and 5). These results demonstrate that the coexistence of the AEL and CPA modes could be realized with an ACM sphere of radius much larger than the incident wavelength. Here, the phase α_1 of the ACM sphere must be $-\pi/2$ or $\pi/2$, which results in a special ACM called pure imaginary materials.

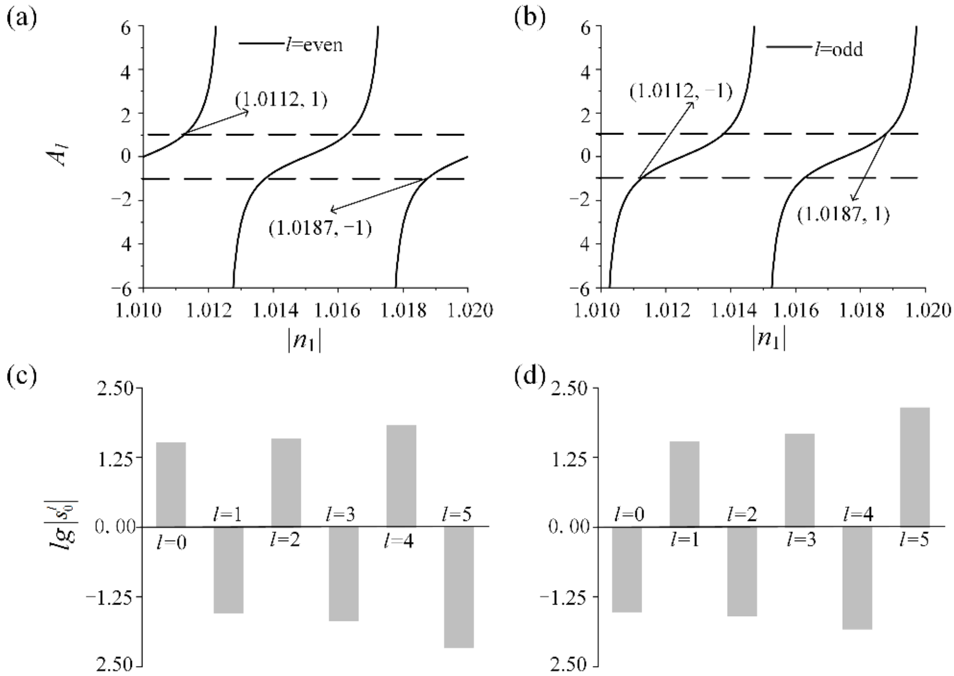

Figure 5. The factor A_l versus the refractive index $|n_1|$ when $R_1 = 100\lambda_0$ for (**a**) even orders l and (**b**) odd orders l. The scattering coefficient $\left|s_0^l\right|$ for different l when $\alpha_1 = -\pi/2$ and $R_1 = 100\lambda_0$ on a logarithmic scale, with (**c**) $|n_1| = 1.0112$ and (**d**) $|n_1| = 1.0187$.

6. AEL and CPA for Multiple Orders Based on a Small Multilayered Sphere

Based on a small monolayer ACM sphere, the AEL or CPA modes are realized, but it can only amplify or absorb spherical wave with a single order l. A monolayer ACM sphere with a radius much larger than the wavelength could simultaneously realize even (or odd) order AEL modes and odd (or even) order CPA modes, but the bulky geometry may limit its potential applications. In order to manipulate spherical waves with multiple channel orders simultaneously, a multilayered ACM sphere is considered because it contains material parameters with more degrees of freedom. Generally, a multilayered structure consisting of Q layers could simultaneously manipulate spherical waves with total Q orders [46]. Here, a three-layered ACM sphere (Q = 3) is proposed as an example, where the outer radius of each layer is $R_1 = 0.35$ m, $R_2 = 0.25$ m, and $R_3 = 0.15$ m, the incident wavelength is $\lambda_0 = 1$ m, and the refractive indexes of three layers $\left|n_q\right|$ are all set to 2 for simplicity, unless otherwise stated. Then, the scattering coefficient s_0^l can be obtained by iterating Equations (6) and (8).

We first aim to realize the AEL mode for order l = 1 and the CPA modes for orders l = 0 and 2, which requires $s_0^0 = 0$, $s_0^1 \to \infty$, and $s_0^2 = 0$, simultaneously. By numerically solving these three equations, one can finally find the required acoustic parameters of the three-layered ACM sphere as $\rho_1 = (1.5075 + 0.0089i)\rho_0$, $\rho_2 = (-0.1038 + 0.8555i)\rho_0$, and $\rho_3 = (-0.0537 + 0.2748i)\rho_0$, respectively. For a three-layered ACM sphere with such acoustic parameters, Figure 6a–c show the simulated total pressure fields in the yz-plane where spherical waves with orders l = 0, 1 and 2, respectively, are incident on the sphere. For l = 0 (see Figure 6a) and l = 2 (see Figure 6c), the values of the total fields at the outermost simulation boundary $r = \lambda_0$ are close to the corresponding incident pressure $P_l(\cos\theta)$, and no obvious interference pattern is observed in the background medium, indicating the realization of CPA modes for orders l = 0 and 2. In contrast, for l = 1 (see Figure 6b), the total acoustic field in the air is far beyond the incidence field (see color bar), verifying the realization of the AEL mode for order l = 1.

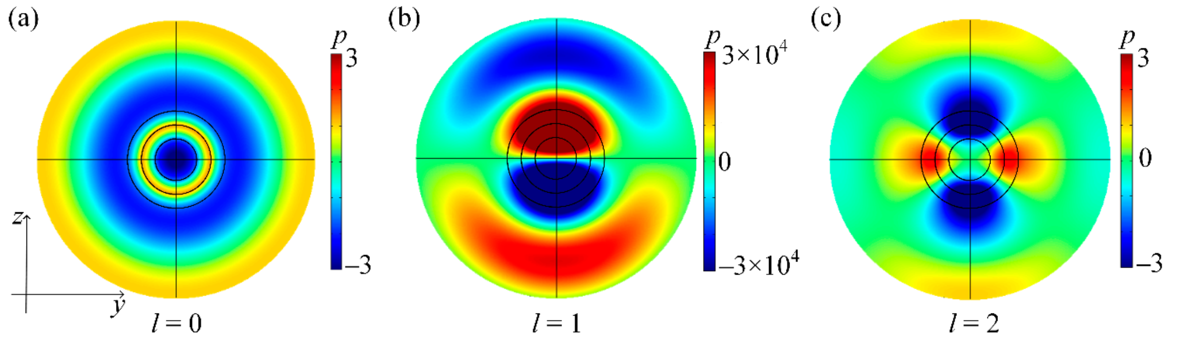

Figure 6. Simulated total acoustic pressure fields of the AEL and CPA modes in the *yz*-plane for spherical wave incidence with different orders l based on a three-layered ACM sphere: (**a**) $l = 0$; (**b**) $l = 1$; (**c**) $l = 2$. In all simulations, $R_1 = 0.35$ m, $R_2 = 0.25$ m, $R_3 = 0.15$ m, $|n_1| = |n_2| = |n_3| = 2$, $\rho_1 = (1.5075 + 0.0089i)\rho_0$, $\rho_2 = (-0.1038 + 0.8555i)\rho_0$, $\rho_3 = (-0.0537 + 0.2748i)\rho_0$, $\lambda_0 = 1$ m, and the distribution of the incident pressure field at the outermost simulation boundary ($r = \lambda_0$) is $P_l(\cos\theta)$.

In addition, the multilayered structure could be designed to manipulate spherical waves with multiple orders at different frequencies f. For the second example, a three-layered ACM sphere is designed to realize a CPA mode with order $l = 0$ at 300 Hz, an AEL mode at 343 Hz for $l = 1$, and a CPA mode at 400 Hz for $l = 2$. By solving $s_0^0 = 0$ at 300 Hz, $s_0^1 \to \infty$ at 343 Hz, and $s_0^2 = 0$ at 400 Hz simultaneously, it can be obtained that $\rho_1 = (1.0810 - 1.7525i)\rho_0$, $\rho_2 = (0.1611 - 2.5259i)\rho_0$, and $\rho_3 = (-0.1425 + 0.2342i)\rho_0$, respectively. The corresponding simulated results are shown in the upper panels of Figure 7a–c. For $l = 0$ (see Figure 7a), the acoustic field is independent of θ, while for $l = 2$ (see Figure 7c), the acoustic intensity is strong along the y and z-axes. In both cases, the values at the outermost simulation boundary $r = 1$ m are very close to the corresponding setting incidence pressure $P_l(\cos\theta)$, and no obvious interference pattern is observed. Therefore, the CPA modes are realized for two orders at two frequencies. For $l = 1$ (see Figure 7b), the acoustic intensity is maximal along the z-axis and minimal along the y-axis. In addition, the total field far exceeds the incidence, i.e., the AEL mode occurs.

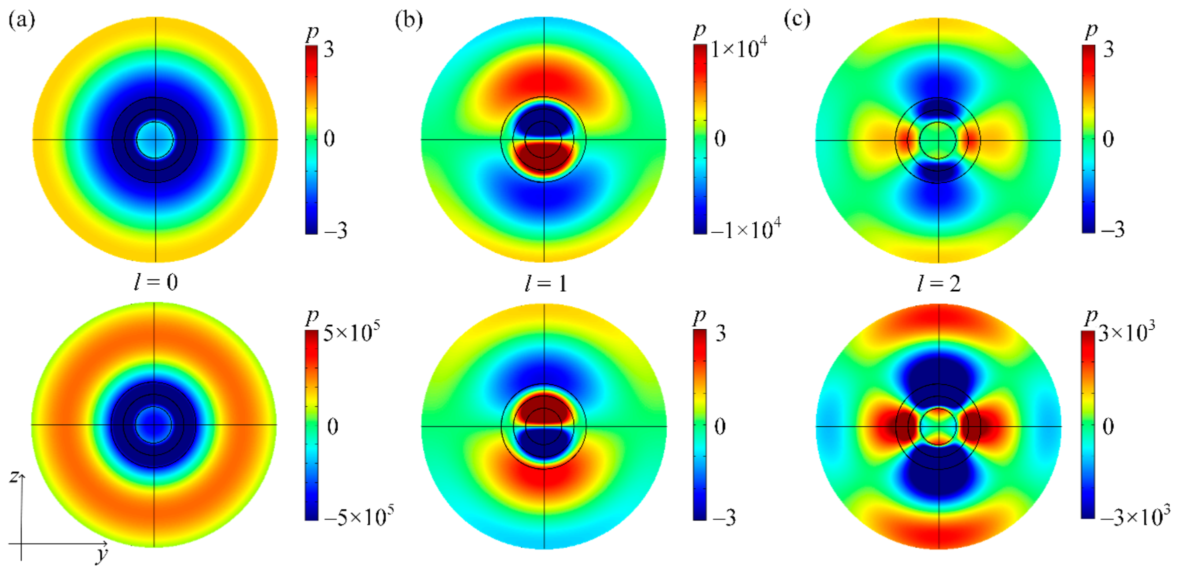

Figure 7. Simulated total acoustic pressure fields of the AEL and CPA modes in the *yz*-plane for spherical wave incidence with different orders l at different incidence frequencies f based on a three-

layered ACM sphere. (**a**) l = 0 and f = 300 Hz. (**b**) l = 1 and f = 343 Hz. (**c**) l = 2 and f = 400 Hz. For the upper panels, the acoustic parameters are $\rho_1 = (1.0810 - 1.7525i)\rho_0$, $\rho_2 = (0.1611 - 2.5259i)\rho_0$, and $\rho_3 = (-0.1425 + 0.2342i)\rho_0$, while for the lower panels, $\rho_1 = (1.0810 + 1.7525i)\rho_0$, $\rho_2 = (0.1611 + 2.5259i)\rho_0$, and $\rho_3 = (-0.1425 - 0.2342i)\rho_0$. In all simulations, $R_1 = 0.35$ m, $R_2 = 0.25$ m, $R_3 = 0.15$ m, $|n_1| = |n_2| = |n_3| = 2$, and the distribution of the incident pressure field at the outermost simulation boundary (r = 1 m) is $P_l(\cos\theta)$.

It is worth noting that since the AEL and CPA modes are each other's time reversal counterparts, the time reversal results can be achieved by changing the sign of the imaginary acoustic parameters. For example, a three-layered ACM sphere with $\rho_1 = (1.0810 + 1.7525i)\rho_0$, $\rho_2 = (0.1611 + 2.5259i)\rho_0$, and $\rho_3 = (-0.1425 - 0.2342i)\rho_0$ can realize an AEL mode at 300 Hz for l = 0, a CPA mode at 343 Hz for l = 1, and an AEL mode at 400 Hz for l = 2. The corresponding simulations are shown in the lower panels of Figure 7a–c, which are the time reversal patterns of those in the upper panels of Figure 7a–c. That is, all simulation parameters are the same as those of the upper panels, except that the acoustic parameters for the lower panels are complex conjugates with those for the upper panels. As expected, the AEL mode at 300 Hz for l = 0, the CPA mode at 343 Hz for l = 1, and the AEL mode at 400 Hz for l = 2 are all achieved.

7. Conclusions

In conclusion, we explore the extraordinary scattering properties of a 3D ACM sphere, which possesses both loss and gain, under spherical wave incidence with different orders l. It is found that the AEL and CPA modes could be realized by using an ACM sphere. When the radius of the ACM sphere is far beyond the incidence wavelength, extreme amplification and total absorption for spherical waves with even (or odd) orders and odd (or even) orders can be realized simultaneously. For a small monolayer ACM sphere, only the AEL or CPA mode for a fixed order l can be achieved. Therefore, the multilayered ACM sphere is further considered to realize manipulation on spherical waves with multiple orders. The proposed ACM spheres may provide an alternative method to design acoustic functional devices, such as amplifiers and absorbers.

Author Contributions: Conceptualization, Q.W. and D.-J.W.; funding acquisition, Q.W., X.-F.Z., J.Y. and D.-J.W.; investigation, X.-X.M., Q.W. and D.-J.W.; project administration, Q.W. and D.-J.W.; writing—original draft, X.-X.M. and Q.W.; writing—review and editing, Q.W., X.-F.Z., J.Y. and D.-J.W. All authors have read and agreed to the published version of the manuscript.

Funding: This research was funded by the National Natural Science Foundation of China (NSFC) (under Grant Nos. 12027808, 11874222, 12074191, 12174197, and 11704192).

Institutional Review Board Statement: Not applicable.

Informed Consent Statement: Not applicable.

Conflicts of Interest: The authors declare no conflict of interest.

References

1. Liu, Z.Y.; Zhang, X.X.; Mao, Y.W.; Zhu, Y.Y.; Yang, Z.Y.; Chan, C.T.; Sheng, P. Locally resonant sonic materials. *Science* **2000**, *289*, 1734–1736. [CrossRef] [PubMed]
2. Cummer, S.A.; Christensen, J.; Alù, A. Controlling sound with acoustic metamaterials. *Nat. Rev. Mater.* **2016**, *1*, 16001. [CrossRef]
3. Ma, G.C.; Sheng, P. Acoustic metamaterials: From local resonances to broad horizons. *Sci. Adv.* **2016**, *2*, e1501595. [CrossRef] [PubMed]
4. Fang, N.; Xi, D.J.; Xu, J.; Ambati, M.; Srituravanich, W.; Sun, C.; Zhang, X. Ultrasonic metamaterials with negative modulus. *Nat. Mater.* **2006**, *5*, 452–456. [CrossRef]
5. Assouar, B.; Liang, B.; Wu, Y.; Li, Y.; Cheng, J.-C.; Jing, Y. Acoustic metasurfaces. *Nat. Rev. Mater.* **2018**, *3*, 460. [CrossRef]
6. Landi, M.; Zhao, J.; Prather, W.E.; Wu, Y.; Zhang, L. Acoustic Purcell effect for enhanced emission. *Phys. Rev. Lett.* **2018**, *120*, 114301. [CrossRef]
7. Ao, X.; Chan, C.T. Far-field image magnification for acoustic waves using anisotropic acoustic metamaterials. *Phys. Rev. E* **2008**, *77*, 025601 (R). [CrossRef]

8. Zhu, J.; Christensen, J.; Jung, J.; Martin-Moreno, L.; Yin, X.; Fok, L.; Zhang, X.; Garcia-Vidal, F.J. A holey-structured metamaterial for acoustic deep-subwavelength imaging. *Nat. Phys.* **2011**, *7*, 52. [CrossRef]
9. He, H.; Qiu, C.; Ye, L.; Cai, X.; Fan, X.; Ke, M.; Zhang, F.; Liu, Z. Topological negative refraction of surface acoustic waves in a Weyl phononic crystal. *Nature* **2018**, *560*, 61. [CrossRef]
10. Fan, L.; Mei, J. Metagratings for waterborne sound: Various functionalities enabled by an efficient inverse-design approach. *Phys. Rev. Appl.* **2020**, *14*, 044003. [CrossRef]
11. Liu, Z.Y.; Chan, C.T.; Sheng, P. Analytic model of phononic crystals with local resonances. *Phys. Rev. B* **2005**, *71*, 014103. [CrossRef]
12. Cheng, Y.; Xu, J.Y.; Liu, X.J. Broad forbidden bands in paraller-coupled locally resonant ultrasonic metamaterials. *Appl. Phys. Lett.* **2008**, *92*, 051913. [CrossRef]
13. Yang, Z.; Mei, J.; Yang, M.; Chan, N.H.; Sheng, P. Membrane-type acoustic metamaterial with negative dynamic mass. *Phys. Rev. Lett.* **2008**, *101*, 204301. [CrossRef] [PubMed]
14. Cselyuszka, N.; Sečujski, M.; Crnojević-Bengin, V. Novel negative mass density resonant metamaterial unit cell. *Phys. Lett. A* **2015**, *379*, 33–36. [CrossRef]
15. Cheng, Y.; Zhou, C.; Yuan, B.G.; Wu, D.J.; Wei, Q.; Liu, X.J. Ultra-sparse metasurface for high reflection of low-frequency sound based on artificial Mie resonances. *Nat. Mater.* **2015**, *14*, 1013–1019. [CrossRef]
16. Christensen, J.; Martín-Moreno, L.; García-Vidal, F.J. All-angle blockage of sound by an acoustic double-fishnet metamaterial. *Appl. Phys. Lett.* **2010**, *9*, 134106. [CrossRef]
17. Ding, Y.Q.; Liu, Z.Y.; Qiu, C.Y.; Shi, J. Metamaterial with simultaneously negative bulk modulus and mass density. *Phys. Rev. Lett.* **2007**, *99*, 093904. [CrossRef]
18. Liu, X.N.; Hu, J.K.; Huang, G.L.; Sun, C.T. An elastic mematerial with simultaneously negative mass density and bulk modulus. *Appl. Phys. Lett.* **2011**, *98*, 251907. [CrossRef]
19. Cheng, Y.; Xu, J.Y.; Liu, X.J. One-dimensional structured ultrasonic metamaterials with simultaneously negative dynamic density and modulus. *Phys. Rev. B* **2008**, *77*, 045134. [CrossRef]
20. Pendry, J.B. Negative refraction makes a perfect lens. *Phys. Rev. Lett.* **2000**, *85*, 3966–3969. [CrossRef]
21. Deng, K.; Ding, Y.Q.; He, Z.J.; Zhao, H.; Shi, J.; Liu, Z.Y. Theoretical study of subwavelength imaging by acoustic metamaterial slabs. *J. Appl. Phys.* **2009**, *105*, 124909. [CrossRef]
22. Yang, M.; Ma, G.; Yang, Z.Y.; Sheng, P. Coupled membranes with doubly negative mass density and bulk modulus. *Phys. Rev. Lett.* **2013**, *110*, 134301. [CrossRef] [PubMed]
23. Liang, Z.; Li, J. Extreme acoustic metamaterial by coiling up space. *Phys. Rev. Lett.* **2012**, *108*, 114301. [CrossRef] [PubMed]
24. Xu, C.; Ma, G.; Chen, Z.-G.; Luo, J.; Shi, J.; Lai, Y.; Wu, Y. Three-dimensional acoustic double-zero-index medium with a fourfold degenerate Dirac-like point. *Phys. Rev. Lett.* **2020**, *124*, 074501. [CrossRef]
25. Jing, Y.; Xu, J.; Fang, N.X. Numerical study of a near-zero-index acoustic metamaterial. *Phys. Lett. A* **2012**, *376*, 2834–2837. [CrossRef]
26. Hao, G.M.; Yan, W.; Qiu, M. Super-reflection and cloaking based on zero index metamaterial. *Appl. Phys. Lett.* **2010**, *96*, 101109. [CrossRef]
27. Cselyuszka, N.; Sečujski, M.; Bengin, C.V. Compressibility-nero-zero acoustic metamaterial. *Phys. Lett. A* **2014**, *378*, 1153–1156. [CrossRef]
28. Hu, B.; Zhang, Z.W.; Zhang, H.X.; Zheng, L.Y.; Xiong, W.; Yue, Z.C.; Wang, X.Y.; Xu, J.Y.; Cheng, Y.; Liu, X.J.; et al. Non-Hermitian topological whispering gallery. *Nature* **2021**, *597*, 655–659. [CrossRef]
29. Wang, X.; Fang, X.S.; Mao, D.X.; Jing, Y.; Li, Y. Extremely asymmetrical acoustic metasurface mirror at the exceptional point. *Phys. Rev. Lett.* **2019**, *123*, 214302. [CrossRef]
30. Dong, S.H.; Hu, G.W.; Wang, Q.; Jia, Y.X.; Zhang, Q.; Cao, G.T.; Wang, J.F.; Chen, S.Q.; Fan, D.Y.; Jiang, W.X.; et al. Loss-assisted metasurface at an exceptional point. *ACS Photonics* **2020**, *7*, 3321–3327. [CrossRef]
31. Huang, X.Y.; Lu, C.C.; Liang, C.; Tao, H.G.; Liu, Y.C. Loss-induced nonreciprocity. *Light-Sci. Appl.* **2021**, *10*, 30. [CrossRef] [PubMed]
32. Zhu, X.F.; Ramezani, H.; Shi, C.Z.; Zhu, J.; Zhang, X. PT-Symmetric acoustics. *Phys. Rev. X* **2014**, *4*, 031042. [CrossRef]
33. Dragoman, D. Complex conjugate media: Alternative configurations for miniaturized lasers. *Opt. Commun.* **2011**, *284*, 2095–2098. [CrossRef]
34. Xu, Y.D.; Fu, Y.Y.; Chen, H.Y. Electromagnetic wave propagations in conjugate metamaterials. *Opt. Express* **2017**, *25*, 4952–4966. [CrossRef]
35. Fu, Y.Y.; Cao, Y.Y.; Cummer, S.A.; Xu, Y.D.; Chen, H.Y. Coherent perfect absorber and laser modes in purely imaginary metamaterials. *Phys. Rev. A* **2017**, *96*, 043838. [CrossRef]
36. Fu, Y.Y.; Xu, Y.D.; Chen, H.Y.; Cummer, S.A. Coherent perfect absorption and laser modes in a cylindrical structure of conjugate metamaterials. *New J. Phys.* **2018**, *20*, 013015. [CrossRef]
37. Chen, L.; Fan, L.; Zhang, S.Y. Acoustic conjugate metamaterials. *Phys. Rev. B* **2019**, *100*, 024111. [CrossRef]
38. Song, J.Z.; Bai, P.; Hang, Z.H.; Lai, Y. Acoustic coherent perfect absorbers. *New J. Phys.* **2014**, *16*, 033026. [CrossRef]
39. Ji, W.-Q.; Wei, Q.; Zhu, X.-F.; Wu, D.-J.; Liu, X.-J. Extraordinary acoustic scattering in a periodic PT-symmetric zero-index metamaterials waveguide. *EPL* **2019**, *125*, 58002. [CrossRef]

40. Hu, T.; Wei, Q.; Zhu, X.-F.; Yao, J.; Wu, D.-J. Acoustic anti-parity-time symmetric structure enabling equivalent lasing and coherent perfect absorption. *Phys. Rev. B* **2021**, *104*, 134110. [CrossRef]
41. Baranov, D.G.; Krasnok, A.; Shegai, T.; Alù, A.; Chong, Y.D. Coherent perfect absorbers: Linear control of light with light. *Nat. Rev. Mater.* **2017**, *2*, 17064. [CrossRef]
42. Chong, Y.D.; Ge, L.; Cao, H.; Stone, A.D. Coherent perfect absorbers: Time-reversed lasers. *Phys. Rev. Lett.* **2010**, *105*, 053901. [CrossRef] [PubMed]
43. Wan, W.J.; Chong, Y.D.; Ge, L.; Noh, H.; Stone, A.D.; Cao, H. Time-reversed lasing and interferometric control of absorption. *Science* **2011**, *331*, 889–892. [CrossRef] [PubMed]
44. Longhi, S. PT-symmetric laser absorber. *Phys. Rev. A* **2010**, *82*, 031801. [CrossRef]
45. Wang, H.; Kong, W.; Zhang, P.; Li, Z.; Zhong, D. Coherent Perfect Absorption Laser Points in One-Dimensional Anti-Parity–Time-Symmetric Photonic Crystals. *Appl. Sci.* **2019**, *9*, 2738. [CrossRef]
46. Bai, P.; Wu, Y.; Lai, Y. Multi-channel coherent perfect absorbers. *EPL* **2016**, *114*, 28003. [CrossRef]